Vietnam Journal of Chemistry, International Edition, **55**(4): 521-526, 2017
DOI: 10.15625/2525-2321.2017-00502

Effect of chromium substituted on structural and magnetic characterization lithium ferrite nanoparticles

Nguyen Thi Lan[1*], Phuong Dinh Tam[1], Nguyen Phuong Duong[2], Than Duc Hien[2]

[1]*Advanced Institute for Science and Technology, Hanoi University of Science and Technology (HUST)*

[2]*International Training Institute for Materials Science, HUST*

Received 16 June 2017; Accepted for publication 28 August 2017

Abstract

In this work, we present a structural, morphology and magnetic study of the $Li_{0.5}Fe_{2.5-x}Cr_xO_4$ spinel nanoparticles (x = 0, 0.5, 0.75, 1, and 1.25) with mean particle size of 20-30 nm prepared by sol-gel method. The lattice constants and the size of particle decrease with increasing Cr concentration. In these samples, the preference of Cr^{3+} and Li^+ ions in the octahedral sites and a small degree of site-interchange between Li^+ in the octahedral sites and Fe^{3+} in the tetrahedral sites were found which increases with increasing the Cr content. A decrease of magnetization due to the spin disorder in the surface layer of the particles was observed. The spontaneous magnetization at 5K suggests the Néel type of magnetic ordering in these samples. The magnetic coercivity is discussed in terms of particle size, morphology and chromium substitution.

Keywords. Chromium substitution, sol-gel method, nanoparticles, lithium ferrite.

1. INTRODUCTION

Lithium ferrite $Li_{0.5}Fe_{2.5}O_4$ possesses high saturation magnetization, high Curie temperature and soft magnetic hysteresis loop. For a long time it has continuously been interested for application in the fields of low-cost microwave devices, memory cores [1, 2] and for cathode materials in rechargeable lithium batteries [3]. $Li_{0.5}Fe_{2.5}O_4$ is an inverse spinel with the Li^+ and the three-fifths of the Fe^{3+} ions occupying the octahedral B sites of the cubic spinel structure of the general formula AB_2O_4. The rest of the Fe^{3+} ions are located at the tetrahedral A sites.

The substitution of other 3*d* ions for iron plays an important role on the modifications of the site occupancy as well as on the electrical and magnetic properties of lithium ferrite [4]. Among others, chromium substituted lithium ferrites have been the subject of extensive technical and fundamental investigation through the years. Several groups performed Mössbauer experiments in order to specify the cation distribution at *A* and *B* sites of $Li_{0.5}Fe_{2.5-x}Cr_xO_4$ ($0 \le x \le 2$) samples prepared by different techniques [5-9]. A general conclusion is that Cr^{3+} has a strong tendency to occupy *B* site by replacing Fe^{3+} ions because of favorable crystal field effects. With a successive increases of Cr^{3+}, Li^{1+} ions are driven to the *A* site to satisfy the charge compensation condition. The crystal structure shifts from order to disorder form up on chromium substitution [6, 7]. Thereby, the nominal cation distribution in the $Li_{0.5}Fe_{2.5-x}Cr_xO_4$ series can be summarized as in table 1.

One of the known effects of substitution by Cr is to disrupt the interatomic exchange interactions between Fe^{3+} ions and hence the Curie point decreases monotonously with Cr content x. On the other hand, the chromium substituted lithium ferrites are among the few systems exhibiting the effect of magnetic compensation which was first pointed out by Gorter [10]. However, irregular distribution of cations in the two crystallographic sites often take place in ferrite nanoparticles prepared at lower sintering temperatures in comparison with the conventional ceramic method. Dey et al. have characterized the $Li_{0.5}Fe_{2.5}O_4$ nanoparticles prepared by citrate precursor method and showed that in the preparation process the formation of a gel followed by spongy mass may lead to random distribution of Li^+ between the octahedral and tetrahedral sites during sintering of the samples [11]. The authors have shown that the number of Li^+ ions in the tetrahedral sites is 0.36 and 0.34 ions per formula unit for the samples with average particle diameter of 9.9 nm and 19.4 nm, respectively. The change in cation distribution leads to substantial modifications

of magnetic properties such as sublattice moments, magnetic interactions and anisotropy.

Although many works have been reported on the preparation and characterization of the $Li_{0.5}Fe_{2.5-x}Cr_xO_4$ in bulk and nanosized forms, there is a lack of neutron scattering and magnetization data at low temperatures which are helpful for the discussion of magnetic ordering in these materials. This paper presents the study of crystal structure and the magnetization of the $Li_{0.5}Fe_{2.5-x}Cr_xO_4$ ($0 \le x \le 1$) nanoparticles prepared by a citrate sol-gel route. The motivation for the study on the nanoparticle samples is due to their relevance to the modern technological applications [12, 13]. Discussions are focused on the size confinement and cation distribution effects toward the spontaneous magnetization, coercivity, and magnetic ordering.

2. EXPERIMENTAL

Stoichoimetric amounts of $LiNO_3$, $Fe(NO_3)_3$, $Cr(NO_3)_3$ were dissolved completely in deionized water. In these processes, $Li^+/[(1-x)Fe^{3+}+xCr^{3+}]$ was fixed at 0.5/2.5 and $xCr^{3+}/(1-x)Fe^{3+}$ was varied with x = 0, 0.5, 0.75, 1 and 1.25. Each aqueous solution containing Li^{1+}, Fe^{3+} and Cr^{3+} was poured into citric acid (AC) with the total cations/citric acid molar ratio = 1/1. Ammonium hydroxide in aqueous form was added to the mixed solutions and the pH of the solutions was adjusted to about 7. The mixtures were stirred at 1000 rpm and slowly evaporated at 80 ^oC to form gels. The gels were dried at 120 ^oC for 2 h and then heated in air at 350 ^oC for 2h in order to form xerogels. The nanoparticle samples were obtained after sintering the products at 600 ^oC in 2h.

X-ray diffraction (XRD, Cu-Kα, Siemens D-5000) was employed to identify the crystal structure of the samples at room temperature. High-resolution transmission electron microscope (Tecnai G2 F30) was used to examine the particle size and morphology. The Fe/Cr ratios at sample surfaces were determined on an X-ray microanalysis system (ThermoNora). The magnetic loops at 5 K were measured using a superconducting quantum interference device (SQUID) by Quantum Design with a maximum field of 5T.

3. RESULTS AND DISCUSSION

3.1. Structure and morphology analysis

X–ray patterns show that all the samples contain only cubic spinel oxide phase (Fig. 1a). Superstructure lines were observed for x = 0 and x = 0.5 which arise from the partial ordering of the lithium sublattice [14]. These lines are largely suppressed for x = 0.75 and vanish at higher levels of chromium substitution. This indicates that Cr^{3+} ions are statistically disordered within the structure and disrupt the ordered lithium arrangement.

The cubic lattice parameter a is determined from the XRD patterns and listed in Table 1. For x = 0, a value of 0.834 nm was found for a, which is comparable to that of the bulk $Li_{0.5}Fe_{2.5}O_4$.[15] A systematic decrease in lattice parameter with increasing chromium substitution is seen which is similar to the results of previous studies of materials prepared by conventional ceramic and other chemical methods [13, 14]. Fig. 1b show the Bragg angle at peak (311) increase with increasing Cr substitution. This variation in unite cell size may be attributed to the ionic radius of six-fold-coordinated Cr^{3+} being smaller (0.064 nm) than that of six-fold-coordinated Fe^{3+} (0.067 nm) [16]. The crystallite size of the nanocrystalline samples was measured from XRD line broadening analysis applying Scherrer's formula [17].

$$d = \frac{k\lambda}{\beta \cos\theta} \quad (1)$$

where d is the mean dimension of the crystallites, λ the wavelength of the X-ray radiation, θ the Bragg angle, k a shape factor taken to be 0.95 and β the peak width measured at half of the maximum intensity. The mean crystallite size d decreases with the increase of x which is probably related to the decrease in the lattice constant. Decreasing tendency of particle size was also observed for other Cr substituted ferrites in the forms of nanoparticles and polycrystalline bulk [16, 18]. However, the mechanism for the grain growth has been proposed and requires further investigation.

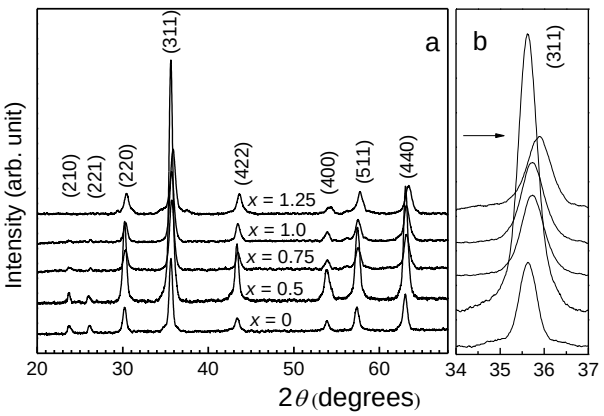

Figure 1: Indexed XRD patterns of the $Li_{0.5}Fe_{2.5-x}Cr_xO_4$ nanoparticle samples

The substitution of other 3*d* ions for iron plays an important role on the modifications of the site occupancy as well as on the electrical and magnetic properties of lithium ferrite [4]. Among others, chromium substituted lithium ferrites have been the subject of extensive technical and fundamental investigation through the years. Several groups performed Mössbauer experiments in order to specify the cation distribution at *A* and *B* sites of $Li_{0.5}Fe_{2.5-x}Cr_xO_4$ ($0 \leq x \leq 2$) samples prepared by different techniques [5, 6, 8, 10, 15]. A general conclusion is that Cr^{3+} has a strong tendency to occupy *B* site by replacing Fe^{3+} ions because of favorable crystal field effects. With a successive increase of Cr^{3+}, Li^{1+} ions are driven to the *A* site to satisfy the charge compensation condition. The crystal structure shifts from order to disorder form up on chromium substitution [6, 10]. Thereby, the nominal cation distribution in the $Li_{0.5}Fe_{2.5-x}Cr_xO_4$ series can be summarized as in Table 1.

Table 1: Nominal composition (using a notation where round brackets denote tetrahedral sites and square brackets denote octahedral sites), the lattice constant a and average crystallite size d of the $Li_{0.5}Fe_{2.5-x}Cr_xO_4$ nanoparticles

x	Nominal composition	*a* (nm)	*D* (nm)
0	$(Fe_1)[Li_{0.5}Fe_{1.5}]O_4$	0.834	29.9
0.5	$(Fe_1)[Li_{0.5}Fe_1Cr_{0.5}]O_4$	0.833	26.9
0.75	$(Fe_1)[Li_{0.5}Fe_{0.75}Cr_{0.75}]O_4$	0.832	25.1
1.0	$(Fe_1)[Li_{0.5}Fe_{0.5}Cr_1]O_4$	0.831	21.9
1.25	$(Fe_1)[Li_{0.5}Fe_{0.25}Cr_{1.25}]O_4$	0.829	21.08

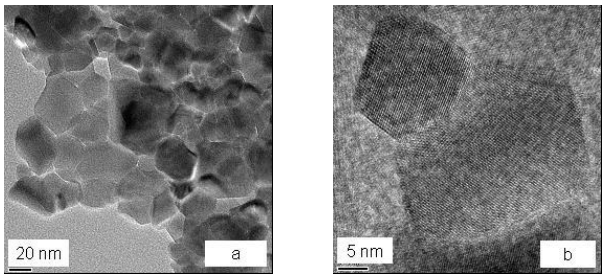

Figure 2: HR-TEM photographs of the sample x = 1.0 in magnification scales 20 nm (a) and 5 nm (b)

The representative HR-TEM photographs of the ensembles *x* = 1 are shown in Fig. 2. Via high-resolution HR-TEM experiments, the well-ordered crystallographic planes in an individual particle of the samples are observed. The particles have polyhedral shapes with particles size in the range of 12-50 nm. Due to the sintering step, some parts of the samples are composed of interconnected particles. The derived average particle sizes of the samples 20.7 nm are comparable to the average crystallite sizes calculated from XRD line broadening. In addition, the element analyses reveal that the Cr/Fe ratios of the substituted samples are very close to the stoichiometries.

3.2. Magnetization loops at 5 K

In order to study the magnetization process in the ground state, the hysteresis loops were measured at 5 K after cooling the samples in zero field. The data are plotted in Fig. 3a. The M–μ_0H curve of the samples approaches to saturation around 1 T and with further increase of magnetic field it is accompanied by a linear high-field susceptibility χ_{HF} (table 2). The spontaneous magnetization M_s was derived by extrapolating the linear part of the curve to zero field. The Fig. 3b shows the loop of the sample x = 0.75 at the low field from which the coercivity H_c is determined. The experimental data of these samples are listed in table 2. For comparison, also shown is the Néel magnetic moment $M_s^{Néel}$ which is the difference of the magnetic moments of *A* and *B* sublattice, i.e. $M = M_B - M_A$ for nominal compositions with spin-only cation moments. As plotted in Fig. 4, the M_s decreases almost proportionally with the increase of Cr content *x*. These results correspond to collinear spin structures where the Cr^{3+} ions of lower spin substitute successively for the Fe^{3+} ions in the *B* sublattice of the dominant magnetic moment.

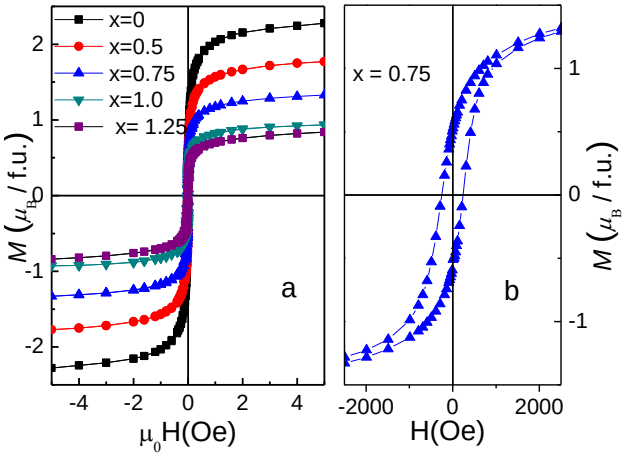

Figure 3: The hysteresis loops of the fixed $Li_{0.5}Fe_{2.5-x}Cr_xO_4$ nanoparticles at 5 K (a) and the sample x = 0.75 at the low field (b)

First, we consider the pure lithium ferrite sample. The observed spontaneous magnetization is 2.1 μ_B/f.u. which is smaller than the calculated value

2.5 μ_B/f.u. The reduced value of M_s can be attributed to the surface effects arising from the broken exchange interactions and reduced coordination in the nanosized particles [14]. The contribution of the disordered spins in the surface shell to the total magnetic moment is manifested by the high-field susceptibility χ_{HF}, being dependent on the surface anisotropy. Assuming the core-shell morphology for one nanoparticle in which the magnetically disordered layer has a constant thickness t, the dependence of magnetization of the sample on the particle size d can be expressed by the following equation [19]:

$$M_s(d) = M_s(\text{bulk})(1\text{-}6t/d) \quad (2)$$

where $M_s(d)$ is the spontaneous magnetization for particles of size d. Using the average d value of 30 nm and M_s(bulk) = 2.5 μ_B/f.u. (table 1), t is obtained as 0.8 nm which is comparable to the lattice constant 0.834 nm. The obtained value is within order of magnitude of those reported earlier for other lithium ferrite nanoparticle systems [14, 20].

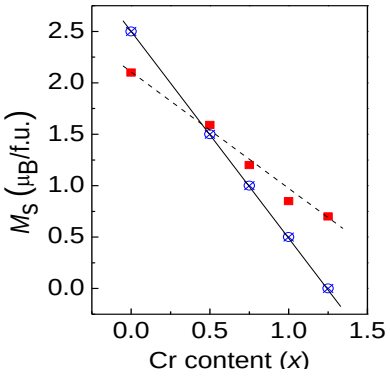

Figure 4: The variations of the spontaneous magnetization M_s at 5 K (■) and the corresponding Néel magnetic moment (○) of the $Li_{0.5}Fe_{2.5-x}Cr_xO_4$ nanoparticles as a function of the Cr content x. Lines are guides to the eyes

On the other hand, the spontaneous magnetizations of the substituted samples are higher than the calculated values which reveal the site-interchange between Fe^{3+} and Li^{1+} in A and B sites, respectively. This result is consistent with the previous studies on the samples with the same composition prepared by the ceramic method [16, 21]. In the work of Gorter et al., [21] it was specified that with increasing Cr content, the proportion of Li^{1+} ions occupying the tetrahedral sites increases which is responsible the imbalance of magnetic moment between A and B sublattices. As mentioned above, M_s is originated from the core part of the particles. The cation distribution was corrected via M_s(bulk) calculated from Eq. (2) where the $M_s(d)$ value, the corresponding particle size and the surface layer thickness (taken as one lattice constant) are input parameters. The number of Li^{1+} ions in the tetrahedral sites in these materials is estimated and listed in table 2.

Table 2: Lithium ion content at the tetrahedral sites, high-field susceptibility χ_{HF}, magnetic coercivity μ_0H_c and spontaneous magnetization M_s of the $Li_{0.5}Fe_{2.5-x}Cr_xO_4$ nanoparticles

x	Li^+ content at A sites (ions/f.u.)	χ_{HF} (10^2 T f.u./μ_B)	μ_0H_c (mT)	M_s (μ_B/f.u.)	$M_s^{Néel}$ (μ_B/f.u.)
0	0	4.50	25	2.10	2.5
0.50	0.048	3.40	24	1.59	1.5
0.75	0.050	2.62	22	1.20	1.0
1.00	0.056	1.96	31	0.85	0.5
1.25	0.090	2.60	25.5	0.70	0.0

The values of $M_s^{Néel}$ calculated based on the Néel model (= $M_B - M_A$) with the spin-only cation moments are also shown.

From the hysteresis loops, the magnetic coercivity H_c of the samples are determined and illustrated in table 2. Generally, for the nanoparticles of soft ferrites, 30-40 nm is the critical size below which the particles are within the range of single domain size limit. The TEM results in Fig. 2 show that the samples in our study are composed of both dispersed particles and interconnected particles due to the sintering process, of which the former corresponds to single domain state and the latter corresponds to the multidomain state. For single domain particle the magnetization process proceeds by coherent rotation of magnetic moment at high applied magnetic fields following the Stoner-Wohlfarth behavior whereas for multidomain particle, domain wall motion dominates. According to magnetism theory [22], in the case of a uniaxial anisotropy material with first order anisotropy constant $K_1 < 0$, the coercivity of an aggregate of single domain particles can be estimated as $H_c = |K_1|/M_s$ whereas for the aggregate of particles with a multidomain structure, $H_c = 0.24|K_1|/M_s$. Thus their coercivity is expected to be between $0.24|K_1|/M_s$ and $|K_1|/M_s$ [22]. Indeed, the coercivity of the pure lithium ferrite sample $x = 0$ (μ_0H_c = 25 mT) lies in between the coercivity limits ($|K_1|/M_s$ ~ 660 Oe) as estimated by using the reported K_1 and M_s values of

$Li_{0.5}Fe_{2.5}O_4$ [4, 22].

The H_c values of the samples fluctuate between 21.3 and 31 mT and do not follow a certain tendency when *x* increases from 0 to 1.25. It should be noted that the coercivity depends on the particle size and morphology of the samples but also on other sources such as $|K_1|$, M_s, long-range dipolar coupling and short-range exchange interaction of interconnected particles. The influence of chromium substitution on the magnetic anisotropy of Cr substituted lithium ferrites was investigated for low Cr concentrations $x \leq 0.4$ [16, 18], which showed the reduction of $|K_1|$ upon chromium substitution.

The samples prepared lithium-chromium nano ferrites of all compositions have the crystallite size from 22 nm and 30 nm. Ferrites with such low particle size are expected to show superparamagnetic behavior. This has motivated the author to investigate the superparamagnetic behavior of these samples by performing Zero Field Cooled (ZFC) and Field Cooled (FC) magnetization measurements using the SQUID.

Figure 5 shows the Magnetization–Temperature curves recorded in FC and ZFC modes for the samples in an external magnetic field of 100 Oe and cooled from 300 K down to 5 K. Phenomenologically, the peak of the ZFC curves corresponds to a state where the particles cross from

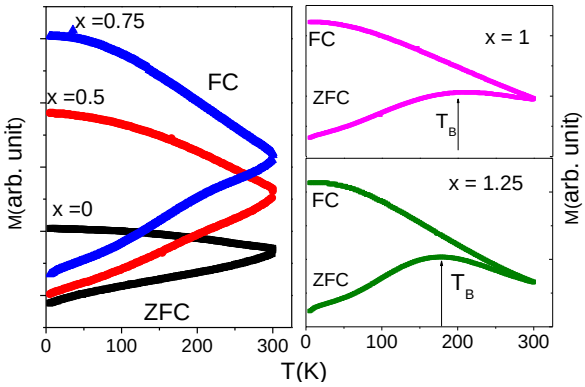

Figure 5: ZFC and FC magnetization curves for the $Li_{0.5}Fe_{2.5-x}Cr_xO_4$ nanoparticle samples measured in an applied field of 100 Oe

superparamagnetic behavior to ferromagnetic behavior with decreasing temperature. The temperature at which this peak occurs is commonly referred to as the blocking temperature. As seen in Fig. 5, at low temperatures the magnetization in the FC curve is higher than that in the ZFC curve and the two curves overlap when the temperature rises above the blocking temperature for the sample *x*=1 and *x* = 1.25, and not appearing in other samples. T_B value is defined from the ZFC-FC curve of the samples *x* = 1 and x = 1.25 in the range 200 K and 180 K, respectively. Caused bythis phenomenon due to the Fe ions be replaced with chromium ions, resulting nanoparticle size is reduced. The critical particle size limit for superparamagnetism decreased with increasing concentrations of Cr

4. CONCLUSION

$Li_{0.5}Fe_{2.5-x}Cr_xO_4$ spinel nanoparticles (x = 0, 0.5, 0.75, 1 and 1.25) were obtained by using a citrate sol-gel method. The samples have the cubic spinel structure at room temperature with the lattice constant *a* slightly decreases with increasing Cr content. The good crystallinity single domain particles has average diameter 22-30 nm. The core-shell model was applied for the nanoparticles in order to estimate the contribution of the spin disorder at the surface layer to the net magnetization, indicating an average surface thickness of 0.8 nm. Magnetic data reveal a small amount of Li^{1+} ions in the B sites interchanges with Fe^{3+} ions in the A sites and the possible collinear ferrimagnetic order for all the samples. The variation of the magnetic coercivity of the particle assemblies as a function of Cr content is qualitatively explained in terms of the model for an aggregate mixture of uniaxial anisotropic single- and multidomain particles and other factors including the anisotropy, saturation magnetization, and interparticle interactions.

Acknowledgment. *The work was supported by Foundation of HUST for Science and Technology Development through a research project (Code: T2016-PC-012).*

REFERENCES

1. A. Goldman. *Modern Ferrite Technology* 2nd Ed. Springer Science, Pittsburgh, PA, USA (2006).
2. J. Nicolas. *Microwave ferrites, Ferromagnetic Materials* Vol. 2, Chapter 3 ed. E.P. Wohlfarth, North Holland (1980).
3. P. Poizot, S. Laruelle, S. Grugeon, L. Dupont and J. M. Tarascon. *Nano-sized transition-metal oxides as negative-electrode materials for lithium-ion batteries*, Nature, **407**, 496-499 (2000).
4. S. Krupička and P. Novák. *Oxide spinels, Ferromagnetic Materials* Vol. 3, Chapter 4 ed. E.P. Wohlfarth, North Holland (1980).
5. N. K. Gill and R. K. Puri. Spectrochim. Acta A. **41**, 1005 (1985).

6. J. L. Dormann, A. Thomas and M. Nogues, Phys. Stat. Sol. (a), **77**, 611 (1983).
7. M. V. Kuznetsov, Q. A. Pankhurst and I. P. Parkin. *Self-propagating high-temperature synthesis of lithium-chromium ferrites* $Li_{0.5}Fe_{2.5-x}Cr_xO_4$, J. Phys D: Appl. Phys., **31**, 2886 (1998).
8. H. Yang, L. Shen, L. Zhao, L. Song, J. Zhao, Z. Wang, L. Wang, D. Zhang. *Magnetic properties of nanocrystalline* $Li_{0.5}Fe_{2.1}Cr_{0.4}O_4$ *ferrite*, Mater. Lett., **57**, 2455 (2003).
9. A. Rais, A. M. Gismelseed and I.A. Al-Omari. *On the magnetic compensation effect of lithium-chromium ferrites* $Li_{0.5}Cr_xFe_{2.5-x}O_4$ $(0 \leq x \leq 1.55)$, Phys. Stat. Sol. (b), **242**, 2949 (2005).
10. S. Dey, A. Roy, D. Das, J. Ghose, *Preparation and characterization of nanocrystalline disordered lithium ferrite by citrate precursor method*, J. Magn. Magn. Mater., **270**, 224 (2004).
11. Q. A. Pankhurst, J. Connolly, S. K. Jones and J. Dobson, *Applications of magnetic nanoparticles in biomedicine*, J. Phys. D, **36**, R167 (2003).
12. M. Shinkai, *Functional magnetic particles for medical application*, J. Biosci. Bioeng., **94**, 606 (2002).
13. S. Verma and P. A. Joy, *Magnetic properties of superparamagnetic lithium ferrite nanoparticles*, J. Appl. Phys., **98**, 124312 (2005).
14. K. P. Chae, Y. B. Lee, J. G. Lee, S. H. Lee. *Crystallographic and magnetic properties of* $CoCr_xFe_{2-x}O_4$ *ferrite powders*, J. Magn. Magn. Mater., **220**, 59 (2000).
15. B. D. Cullity. *Elements of X-Ray Diffraction*, 2nd ed. Addison-Wesley, Reading, MA, 1978.
16. P. N. Vasambekar, C. B. Kolekar, A. S. Vaingankar. *Cation distribution and susceptibility study of Cd–Co and* Cr^{3+} *substituted Cd–Co ferrites*, J. Magn. Magn. Mater., **186**, 333 (1998).
17. J. P. Chen, C. M. Sorensen, K. J. Klabunde, G. C. Hadjipanayis, E. Devlin and A. Kostikas. *Size-dependent magnetic properties of* $MnFe_2O_4$ *fine particles synthesized by coprecipitation*, Phys. Rev. B, **54**, 9288 (1996).
18. E. W. Gorter and J. A. Schulkes. *Reversal of Spontaneous Magnetization as a Function of Temperature in LiFeCr Spinels*, Phys. Rev., **89**, 487 (1953).
19. A. M. Samy, A. A. Sattar, Ibrahim Hassan Afify. *Effect of substitution with potassium and chromium oxides on the magnetic and electrical properties of Li-ferrite*, J. Alloy. Comp., **505**, 297-301 (2010).

Corresponding author: **Nguyen Thi Lan**
Advanced Institute for Science and Technology
Hanoi University of Science and Technology
No. 1, Dai Co Viet Road, Hai Ba Trung Dist., Hanoi
E-mail: lanchoac@gmail.com or lan.nguyenthi1@hust.edu.vn.